



Comparison of the Homogeneous Relaxation Model and a Rayleigh Plesset Cavitation Model in Predicting the Cavitating Flow Through Various Injector Hole Shapes

2013-01-1613
Published
04/08/2013

Federico Brusiani, Sergio Negro and Gian Marco Bianchi
University of Bologna

Maryam Mouhai, Kshitij Neroorkar and David Schmidt
University of Massachusetts-Amherst

Copyright © 2013 SAE International
doi:10.4271/2013-01-1613

ABSTRACT

Two cavitation models are evaluated based on their ability to reproduce the development of cavitation experimentally observed by Winklhofer et al. inside injector hole geometries. The first is Singhal's model, derived from a reduced form of the Rayleigh-Plesset equation, implemented in the commercial CFD package Fluent. The second is the homogeneous relaxation model, a continuum model that uses an empirical timescale to reproduce a range of vaporization mechanisms, implemented in the OpenFOAM framework. Previous work by Neroorkar et al. validated the homogeneous relaxation model for one of the nozzle geometries tested by Winklhofer et al. The present work extends that validation to all the three geometries considered by Winklhofer et al in order to compare the models' ability to capture the effects of nozzle convergence.

As showed by the comparison between numerical and experimental data, both considered cavitation models well predict the effect of nozzle convergence on mass flow rate and the onset of cavitation and choking. However, they show lack of accuracy in reproducing vapor and flow velocity distributions. This may be due to condensation effects, assumptions regarding momentum transfer between phases, and the inadequacy of existing turbulence models for cavitating conditions.

INTRODUCTION

Today, the automotive industry's main concern is improving engine efficiency in order to meet emission targets for HC, CO, NOx, and CO₂ [1]. Gasoline direct injection and Diesel common rail have the potential to increase fuel efficiency and reduce exhaust emissions, but this requires improved spray stability and control of spray characteristics.

Many researchers have turned their attention to the study of nozzle internal flow, finding that there is a close relationship between injector internal geometry and the ensuing spray. In detail, cavitation and flash boiling in the nozzle tip and injector hole volumes have been recognized as two of the most important factors influencing overall spray characteristics [2, 3, 4, 5, 6, 7], with cavitation generally having a positive effect on droplet atomization [4] and a negative effect on spray stability [5] and injector lifetime [6].

The numerical representation of cavitation and flash boiling is still an important area of research due to the difficulties of representing their physics by robust and accurate numerical methodologies. As discussed in Schmidt et al. [8], various models have been suggested for representing the phase change process.

A common Eulerian approach to simulate cavitation is based on the Rayleigh-Plesset equation, which describes the growth and collapse of a bubble in a liquid assuming no slip between the two phases [9]. The Singhal et al. [10] and the Zwart et al. [11] models are two of the most common two phase flow models of this type.

In [12], Neroorkar et al. presented an alternative approach to simulate cavitation based on the homogeneous relaxation model, a continuum flash boiling model which uses an empirical time scale to account for thermal non-equilibrium. Despite the differences between cavitation, which is driven by pressure, and flash boiling, which is also driven by temperature, they are sufficiently similar to suggest that the homogeneous relaxation model can also model cavitation. The results reported in [12] demonstrated the model's ability to correctly reproduce the cavitation observed in one of the geometries experimentally evaluated by Winklhofer et al. [16].

The present work extends the validation presented in [12] to all three geometries tested by Winklhofer et al. in order to evaluate the homogenous relaxation model's ability to capture the effect of nozzle convergence on mass flow rate and the onset of cavitation and choking. The model was implemented in the OpenFOAM framework (HRMFoam). The geometries were also modeled using the Singhal et al. approach in Fluent in order to compare the performance of both models. All the performed simulations were done by adopting RANS approach. Turbulence effects were reproduced by adopting the conventional $k-\epsilon$ turbulence model.

CAVITATION MODELS

Both models are based on the assumption that the vapor and liquid phases are perfectly mixed, which is a good assumption for both cavitation [18] and flash boiling [19,20,21,22]. The mixture is therefore treated as a single fluid with properties averaged between the two phases.

Singhal Cavitation Model

The Singhal et al. [10] cavitation model is formulated using a homogeneous flow approach and takes into account all first order effects of a multiphase flow: phase change, bubble dynamics, turbulent pressure fluctuations, and non-condensable gases. The fluid density (ρ) is a function of the vapor mass fraction (f) and the relationship between them is:

$$\frac{1}{\rho} = \frac{f}{\rho_v} + \frac{1-f}{\rho_l} \quad (1)$$

The vapor mass fraction is governed by a transport equation:

$$\frac{\partial}{\partial t}(\rho f) + \nabla \cdot (\rho f \vec{U}) = \nabla \cdot (\Gamma \nabla f) + R_e - R_c \quad (2)$$

where R_c and R_e are the condensation and evaporation rates respectively.

The vapor volume fraction (α) is related to the vapor mass fraction (f) by the following equation:

$$\alpha = f \cdot \frac{\rho}{\rho_v} \quad (3)$$

To derive an expression for the net phase change rate (R), the two-phase continuity equations are written as follows:

Liquid phase:

$$\frac{\partial}{\partial t}((1-\alpha)\rho_l) + \nabla \cdot ((1-\alpha)\rho_l \vec{U}) = -R \quad (4)$$

Vapor phase:

$$\frac{\partial}{\partial t}(\alpha\rho_v) + \nabla \cdot (\alpha\rho_v \vec{U}) = R \quad (5)$$

Mixture:

$$\frac{\partial}{\partial t}(\rho) + \nabla \cdot (\rho \vec{U}) = 0 \quad (6)$$

Combining Eqs. 4, 5, 6 yields a correlation between the mixture density (ρ) and the void fraction (α):

$$\frac{D}{Dt}(\rho) = -(\rho_l - \rho_v) \frac{D}{Dt}(\alpha) \quad (7)$$

The void fraction (α) is a function of bubble number density (n) and bubble radius (R_B):

$$\alpha = n \frac{4}{3} \pi R_B^3 \quad (8)$$

Substituting Eq. 8 into Eq. 7 yields:

$$\frac{D}{Dt}(\rho) = -(\rho_l - \rho_v)(n4\pi)^{\frac{1}{3}}(3\alpha)^{\frac{2}{3}} \frac{D}{Dt}(R_B) \quad (9)$$

To describe the variation of bubble radius over time, Singhal *et al.* started from the generalized form of the Rayleigh-Plesset equation [9]:

$$\begin{aligned} R_B \frac{D^2 R_B}{Dt^2} + \frac{3}{2} \left(\frac{DR_B}{Dt} \right)^2 \\ = \left(\frac{P_B - P}{\rho_l} \right) - \frac{4v_l}{R_B} \dot{R}_B - \frac{2S}{\rho_l R_B} \end{aligned} \quad (10)$$

In the Rayleigh-Plesset equation, P_B represents the vapor bubble pressure and P represents the pressure of the liquid phase surrounding the vapor bubble.

The bubble radius (R_B) can be mainly expressed as a function of the pressure difference between the gas phase inside the bubble and the liquid phase surrounding the bubble itself. For this reason, in Eq. 10 the surface tension term (S), the viscous damping (v_l), and the second-order derivative of R_B can be neglected. In this way, it is possible to simplify the Eq. 10 as follows:

$$R_B \frac{D^2 R_B}{Dt^2} = \left(\frac{P_B - P}{\rho_l} \right) \quad (11)$$

Substituting Eq. 11 into Eq. 9, it is possible to write the final expression for the liquid-vapor phase change rate (R):

$$R = (n4\pi)^{\frac{1}{3}}(3\alpha)^{\frac{2}{3}} \frac{\rho_l \rho_v}{\rho} \left[\frac{2}{3} \left(\frac{P_B - P}{\rho_l} \right) \right]^{1/2} \quad (12)$$

Eq. 12 states that the phase change rate is a function of the liquid density (ρ_l), vapor density (ρ_v), and mixture density (ρ). In the Fluent implementation, P is taken as the cell center pressure while the bubble pressure value (P_B) is equal to the saturation vapor pressure (P_v).

Combining Eq. 2 and Eq. 12, it is possible to get the following simplified equation for vapor transport:

$$\begin{aligned} \frac{\partial}{\partial t} (\rho f) + \nabla \cdot (\rho f \vec{U}) \\ = (n4\pi)^{\frac{1}{3}}(3\alpha)^{\frac{2}{3}} \frac{\rho_l \rho_v}{\rho} \left[\frac{2}{3} \left(\frac{P_B - P}{\rho_l} \right) \right]^{1/2} \end{aligned} \quad (13)$$

The right side of Eq. 13 represents bubble growth ($P_B > P$) and collapse ($P_B < P$).

The only unknown term of Eq. 12 is the bubble number density (n). In Fluent, to avoid the set-up of the n parameter, the phase change rate is rewritten as a function of R_B .

Finally, R_c and R_e can be written in the following forms [10]:

$$R_e = C_e \frac{\sqrt{k}}{\sigma} \rho_l \rho_v \left[\frac{2}{3} \left(\frac{P_v - P}{\rho_l} \right) \right]^{1/2} (1 - f_v) \quad (14)$$

$$R_c = C_c \frac{\sqrt{k}}{\sigma} \rho_l \rho_v \left[\frac{2}{3} \left(\frac{P - P_v}{\rho_l} \right) \right]^{1/2} f_v \quad (15)$$

In Eqs. 14 and 15 k is the turbulent kinetic energy and C_c and C_e are two empirical constant values equal to 0.01 and 0.02 respectively. Singhal *et al.* evaluated these constants by performing computations on sharp-edged orifices [10].

In Eqs. 14-15 P_v is estimated as follows:

$$P_v = \left[P_v + \frac{P'_{turb}}{2} \right] = \left[P_v + \frac{0.39\rho k}{2} \right] \quad (16)$$

HRMFoam Cavitation Model

The nozzle flow is governed by conservation of mass (Eq. 17) and momentum (Eq. 18) [13]:

$$\frac{\partial \rho}{\partial t} + \nabla \cdot (\phi \vec{U}) = 0 \quad (17)$$

$$\frac{\partial \rho \vec{U}}{\partial t} + \nabla \cdot (\phi \vec{U}) = -\nabla p + \nabla \bar{\tau} \quad (18)$$

where ϕ is the mass flux and $\bar{\tau}$ is the shear stress. In [15], Neroorkar and Schmidt derive a pressure equation, Eq. 19, from the continuity equation and a discretized momentum equation:

$$\rho \nabla \cdot \left(\frac{H(U)}{a_p} \right) - \rho \nabla \cdot \frac{1}{a_p} \nabla p + \frac{\partial \rho}{\partial x} |_{p,h} \frac{Dx}{Dt} = 0 \quad (19)$$

Here, a_p is the coefficient of the momentum contribution from the cell in question and $H(U)$ is the sum of contributions from neighboring cells and source terms.

Although the two phases are assumed to be perfectly mixed, they are not in thermal equilibrium and cannot be adequately described by an equation of state. Without a state equation to provide closure, the homogeneous relaxation model relies on the assumption that the instantaneous vapor fraction (x) tends towards the equilibrium vapor fraction (\bar{x}) over an empirical time scale (Θ):

$$\frac{Dx}{Dt} = \frac{\bar{x} - x}{\Theta} \quad (20)$$

The equilibrium vapor fraction is a function of local enthalpy and pressure, and is obtained from a lookup table. The instantaneous vapor fraction is a function of the local and saturated vapor densities, and void fraction (α):

$$x = \alpha \rho_v / \rho \quad (21)$$

The void fraction is in turn a function of the local and saturation densities:

$$\alpha = \frac{\rho_l - \rho}{\rho_l - \rho_v} \quad (22)$$

What remains is to define Θ . Based on Reocreux's "Moby Dick" experiments, Downar-Zapolski proposed the following correlation for pressures exceeding 10 bar [21, 22, 23]:

$$\Theta = \Theta_0 \alpha^{-0.54} \psi^{-1.76} \quad (23)$$

where

$$\psi = \frac{P_{sat} - P}{P_{crit} - P_{sat}} \quad (24)$$

and $\Theta_0 = 3.84 \times 10^{-7}$.

THROTTLE GEOMETRY

The two cavitation models were evaluated against the experimental cases presented by Winklhofer *et al.* [16]. In [16], experimental tests were performed on three quasi-2D throttle geometries with the same length/thickness (1000μm/300μm) and different K-factors. Figure 1 shows the throttle hole geometries "J", "U", and "W". Their dimensions are summarized in Table 1. The progressive narrowing of the throttle outlet correlates to reduced cavitation. For this reason, simulating flows for all three geometries tests a model's ability to capture the relationship between throttle geometry and cavitation.

For all three geometries, the following experimental data were available:

- Mass flow rate versus pressure drop between the inlet and outlet,
- Pressure profile along the throttle middle line at choked mass flow rate condition,
- Pictures showing the evolution of the vapor phase inside the throttle versus pressure drop.

For the "U" configuration, velocity profiles at 53μm and 170μm downstream of the throttle entrance were also available (V_1 and V_2 sampling lines in Figure 1).

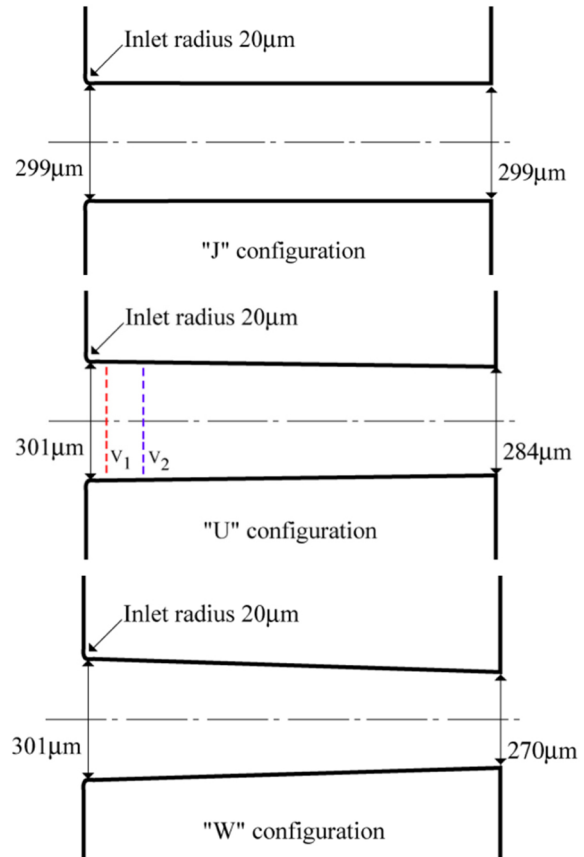


Figure 1. Throttle layout considered in the present paper. For all throttle length and thickness were equal to 1000μm and 300μm respectively.

Table 1. Main geometrical properties characterizing the "J", "U", and "W" injector configurations showed in Figure 1.

Throttle	Inlet		Outlet		Contraction
	radius [μm]	width [μm]	radius [μm]	width [μm]	
"J"	20	299	0	299	0%
"U"	20	301	0	284	5%
"W"	20	301	0	270	10%

SIMULATION SET-UP

Mesh Generation and Boundary Conditions

A 37000 cell 2D unstructured hexahedral mesh was generated for each throttle geometry. Figure 2 shows the mesh structure close to the throttle entrance. Particular care was taken in this area to avoid unphysical results where high fluid dynamic gradients occur. The same mesh was used with both models. The throttle geometries were connected to two additional volumes representing the charge and discharge plenums (Figure 2). The plenums were 4mm in radial direction and 3mm in axial direction.

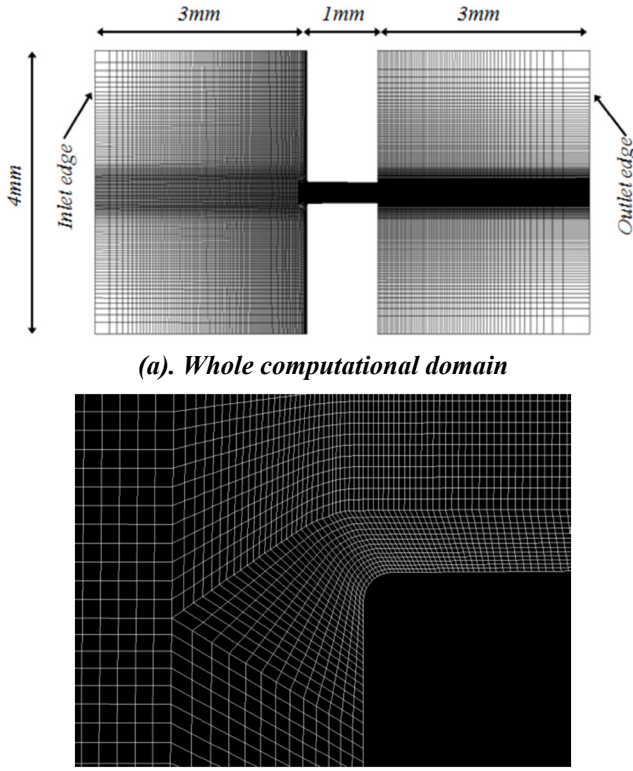


Figure 2. Mesh structure adopted for all the 2D throttle flow case.

Dirichlet conditions for pressure were defined at the inlet-10MPa for all cases-and at the outlet-pressure ranging from 4.5 to 0.5MPa. The increasing pressure drop over the throttle ensured that cavitation would occur for all geometries.

No slip conditions were used for the throttle walls. For both Fluent and HRMFoam simulations the $k-\varepsilon$ turbulence model was used. The initial values for turbulent kinetic energy (k) and dissipation rate (ε) were set on the basis of the following equations:

$$k = \frac{3}{2} (U I)^2 \quad (25)$$

$$\varepsilon = C_\mu^{3/4} \frac{k^{3/2}}{l} \quad (26)$$

where the turbulent intensity I was set to 5%, the turbulent constant C_μ was set to 0.09, and the length scale was set to the 7% of the throttle width [24].

To reproduce the near-wall interaction between fluid flow and wall, the standard wall function model was adopted [25].

Surrogate Diesel Fuel

For all the multiphase simulations performed, the working fluid was the IDEA Diesel fuel surrogate used by Weber et al. [25]. The IDEA fuel is made of 70% n-decane and 30% of α -methylnaphthalene and was implemented in Aspen Plus software which is distributed by AspenTech and used to model chemical engineering processes. The method used for generating surrogates in Aspen Plus and for coupling these properties with HRMFoam are presented by Neroorkar [14]. In Figures 3 and 4 the density and vapor pressure of the IDEA fuel are compared with other industrial Diesel fuels obtained from material safety data sheets (MSDS). The error bars in Figures 3 and 4 show the range of the properties for the industrial fuels. As can be seen, at the working temperature for the considered application ($\sim 31^\circ\text{C}$) the IDEA surrogate physical characteristics are comparable with the other industrial Diesel fuels.

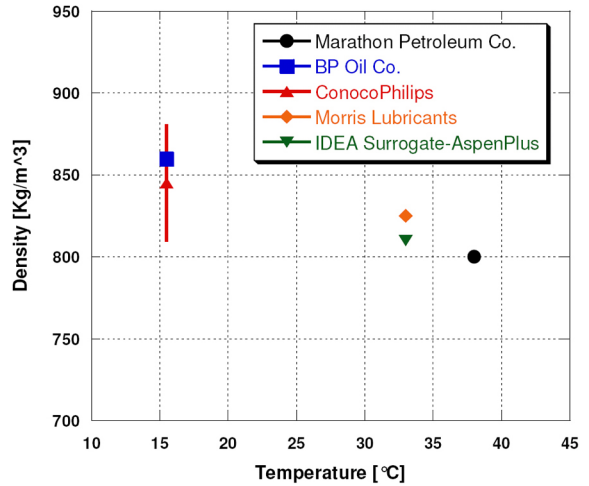


Figure 3. Comparison of the IDEA density with other industrial Diesel fuels.

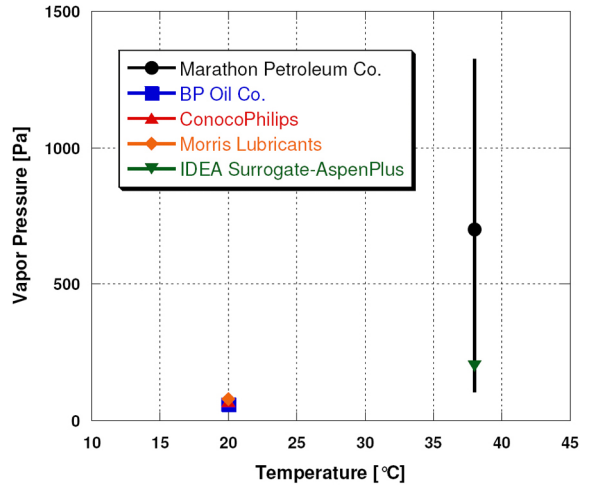


Figure 4. Comparison of the IDEA vapor pressure with other industrial Diesel fuels.

RESULTS AND DISCUSSION

“U” Throttle Geometry

Figure 5 shows the overall hydraulic behavior of throttle “U” in terms of mass flow rate evolution versus pressure difference.

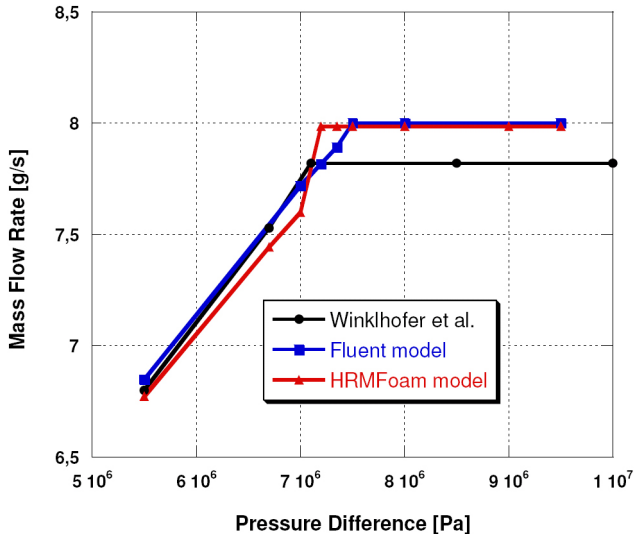


Figure 5. “U” throttle geometry. Mass flow rate evolution versus pressure drops.

In Winklhofer's experiments, the onset of cavitation (CS) occurred when the pressure drop over the throttle was close to 6 MPa [16]. As shown in Figure 6, both cavitation models predicted the experimental location of the incipient vapor formation, but the corresponding CS conditions occurred at 6.7MPa, later than in the experiments. This is expected because the Diesel surrogate adopted for the simulations has a vapor pressure close to 200 Pa while the Diesel used by Winklhofer had a vapor pressure close to 2000 Pa (Figure 5). At the CS condition, the vapor concentration predicted by Fluent model close to the throttle wall was higher than the HRMFoam model.

From the CS condition, increasing the pressure increased the vapor concentration downstream of the throttle inlet. The effect of the cavitation enhancement on the mass flow rate remained slightly evident for both experimental and simulated cases until the cavitation-induced choked flow condition (CC) was reached (Figure 5). As for the CS condition, both models predicted that choking would occur at greater pressure drops than seen in the experimental data. As result, the choked mass flow rates predicted by the numerical models were higher than those observed by Winklhofer (Table 2).

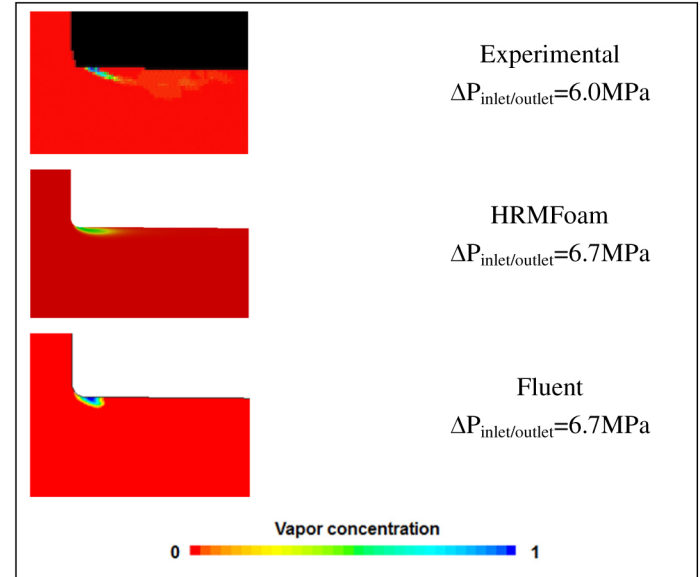


Figure 6. “U” throttle geometry. Experimental and numerical vapor fraction contour observed at CS just downstream the inlet corner.

Table 2. “U” throttle geometry. Comparison between experimental and numerical fluid dynamic conditions at Choking flow condition.

	ΔP@CC [MPa]	Δ%	MF@CC [g/s]	Δ%
Experimental[16]	7	-	7.82	-
HRMFoam model	7.2	+2.8	7.99	+2.2
Fluent model	7.5	+7.1	8.00	+2.3

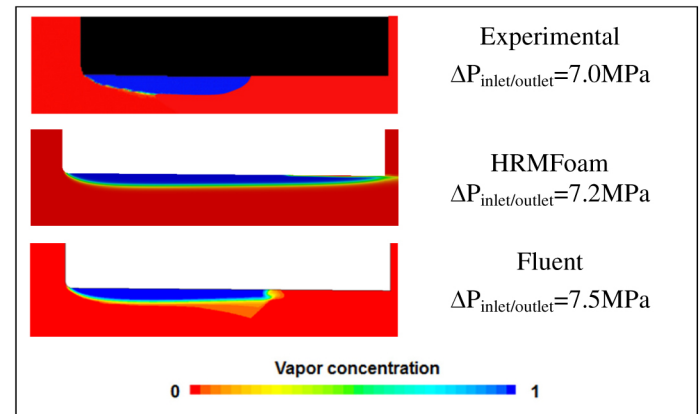


Figure 7. “U” throttle geometry. Numerical vapor fraction contour observed at CC along the throttle axis.

Figure 7 shows that the Fluent model, in agreement with the experimental evidence, predicted that the vapor phase would not reach the throttle outlet under choked flow conditions (CC). The HRMFoam model showed a more evident axial vapor extension. In the 8.5MPa pressure drop case, both models predicted the vapor extension to the outlet (Figure 8).

but neither satisfactorily reproduced the vapor expansion from the nozzle wall to the nozzle axis. However, in comparing the experimental/numerical vapor distributions reported in [Figure 8](#), a significant limitation must be considered: experimentally, the vapor probability distribution was recorded by a CCD camera with back illumination. The difference in light transmittance between liquid and vapor yielded the experimental picture showed in [Figure 8](#). This variable is different from the void fraction contour extracted by computation. Therefore experimental and numerical vapor distributions can only be qualitatively and not quantitatively compared.

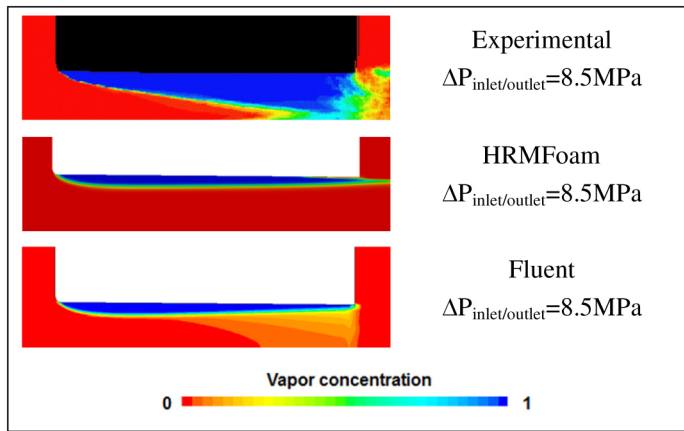


Figure 8. "U" throttle geometry. Experimental and numerical vapor fraction contour observed at pressure drop equal to 8.5MPa.

To complete the comparison between experimental and numerical results, the flow velocity profiles recorded at V_1 and V_2 locations (respectively positioned 53 μm and 170 μm downstream the throttle entrance) were compared.

In detail, [Figures 9](#) and [11](#) compare the flow velocity profiles recorded at V_1 and V_2 locations (53 μm and 170 μm from the throttle inlet, respectively) for three pressure drops:

- 5.5MPa (non-cavitating condition),
- 6.7MPa (onset of cavitation),
- 8.5MPa (choked flow).

All the velocity profiles recorded at V_1 location were characterized by two peaks close to the wall that gradually decrease to a local minimum velocity value at the throttle axis. [Figure 9-a](#) shows this behavior for the 5.5MPa pressure drop case. This is due to the fact that the vapor has a lower density than liquid and, by conservation of momentum, the increased amount of vapor close to the wall led to an increase in the velocity in the near-wall region. [Figure 10](#) shows the computed velocity profile at 5.5MPa of pressure drop. This overall profile was well-reproduced by both models. HRMFoam correctly predicted the minimum and maximum

experimental velocities, albeit with a smoothing of the velocity gradients. This difference between the experimental and HRMFoam velocity gradient distribution produced a shift in the corresponding velocity peak radial positions. Compared to HRMFoam, Fluent more accurately predicted the experimental velocity gradients and the experimental velocity profile in the center of the throttle. Consequently, Fluent's predictions of peak velocity positions were closer to the experimental results, even while overestimating the magnitude of peak velocity ([Figure 9-a](#)). HRMFoam, however, more accurately represented the magnitudes of the peaks.

At the 6.7 MPa pressure drop (onset of cavitation, CS condition), the overall differences in the experimental and predicted velocity profiles remained the same observed for the 5.5MPa pressure drop ([Figure 9-b](#)).

At the 8.5 MPa pressure drop (choked flow) the experimental data shows quite high velocity peaks in the shear layer ([Figure 9-c](#)), mainly due to increased cavitation and the corresponding drop in density which, due to conservation of momentum, increases the velocity of the fluid mixture. Neither model predicted these peaks at choked flow. This may be a consequence of the homogeneous approach, which assumes infinite momentum transfer between phases. This could cause the poor reproduction of velocity gradients in the liquid-vapor transition zone (i.e. the zone where the mismatch between experimental and numerical velocity profiles is more evident). It could also be a consequence of the turbulence model and an unrealistically high energy dissipation rate near the wall.

At V_2 , all the experimental profiles showed progressive increases in velocity until a quasi-constant value was reached between the throttle wall and axis. Then, the velocity increased further, reaching its maximum value at the center of the channel. For the 5.5MPa and 6.7MPa ([Figure 11-a-b](#)) pressure drop cases, both models predicted the near wall velocities and the maximum velocity value close to the channel axis, but neither captured the behavior between the near-wall zone and the central part of the throttle. As with the upstream velocity profiles, this mismatch may be a consequence of the homogeneous flow approach or the choice of turbulence model.

Increasing the pressure drop to 8.5MPa ([Figure 11-c](#)) yielded worse velocity profile predictions close to the center of the throttle. This may be caused by the discrepancies in vapor phase distribution near the throttle axis discussed earlier ([Figure 8](#)).

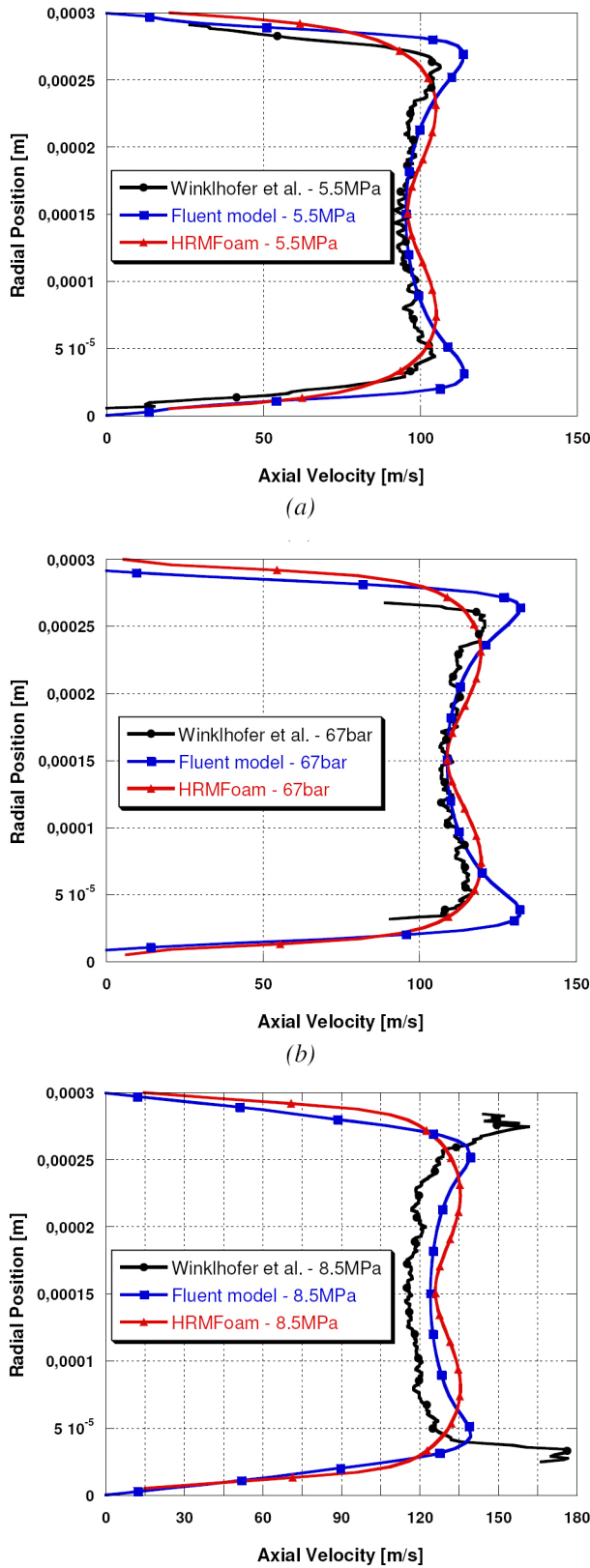


Figure 9. “U” throttle geometry. Comparison of experimental versus simulated velocity profiles at V_1 location for the 5.5MPa, 6.7MPa, and 8.5MPa pressure drops.

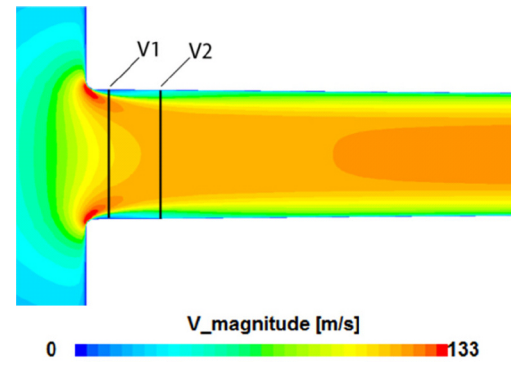


Figure 10. “U” throttle geometry. Flow velocity distribution just downstream the throttle entrance. Pressure drop equal to 5.5MPa pressure drop.

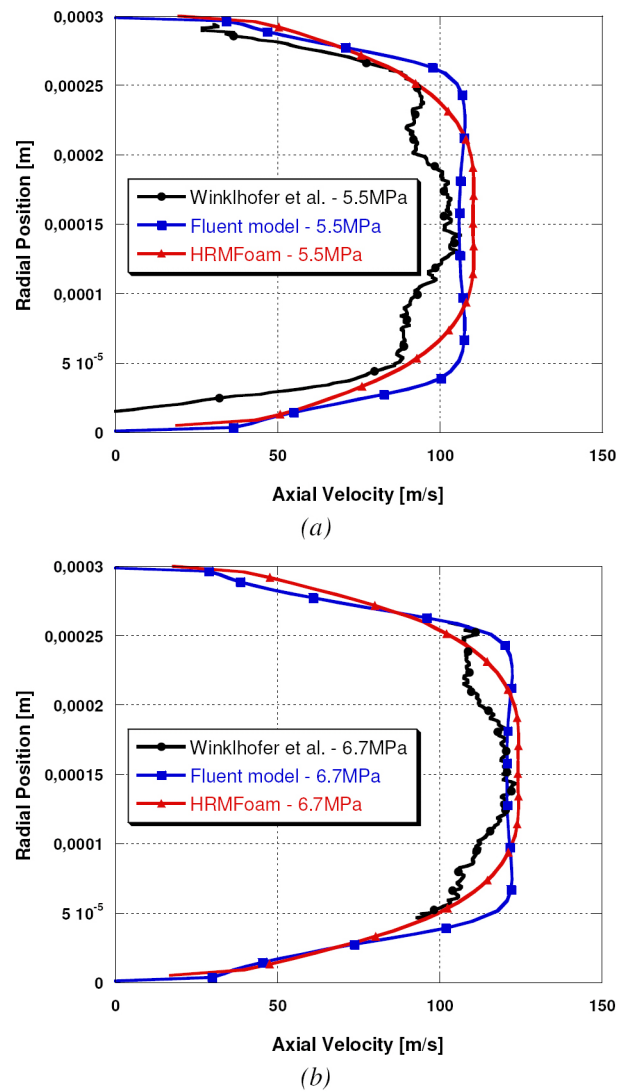


Figure 11. “U” throttle geometry. Comparison of experimental versus simulated velocity profiles at V_2 location at 5.5MPa, 6.7MPa, and 8.5MPa pressure drops.

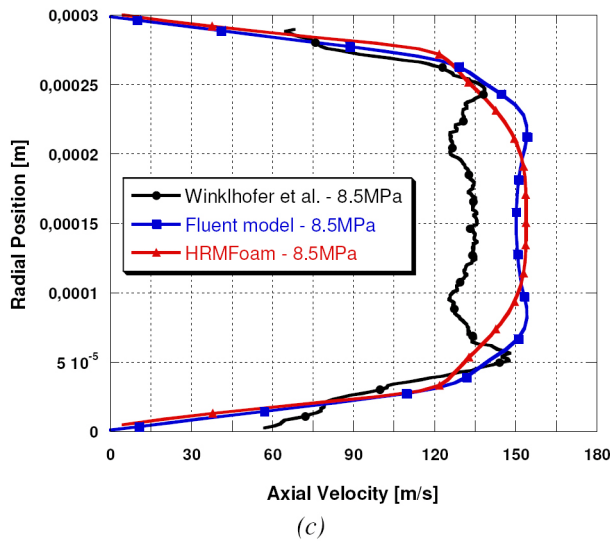


Figure 11. (cont.) “U” throttle geometry. Comparison of experimental versus simulated velocity profiles at V_2 location at 5.5MPa, 6.7MPa, and 8.5MPa pressure drops.

Comparison Between “U”, “J”, and “W” Throttle Configurations

All the above results were obtained for the throttle “U” configuration with a 5% contraction.

In order to evaluate the ability of both models to predict injector performance as a function of the contraction area, the “J” and “W” configurations (Figure 1) were also modeled and compared to Winklhofer et al. [16].

Figure 12 shows the comparison between the experimental mass flow profiles presented in [16] for the three throttle geometries. Based on the experimental mass flow profiles, three effects of increased nozzle contraction were considered:

- Under non-cavitating conditions, the mass flow rate for a given pressure drop should be reduced,
- The onset of choked flow (CC) should be delayed,
- The ultimate choked mass flow rate should not be influenced.

Figure 13 shows that these three characteristics were well-reproduced by both numerical models. Figures 14 and 15 show a good match between experimental and numerical mass flow profiles for the “J” and “W” configurations. Therefore, HRMFoam and Fluent were able to capture mass flow variation as a function of the throttle contraction area.

The experimental results showed that vapor distribution at the onset of cavitation was only slightly influenced by the degree of contraction. Figure 16 shows that, in agreement with experimental evidence, both cavitation models predicted the onset of cavitation for the “J” configuration at only a slightly lesser pressure drop than for the “U” and “W” configurations. Furthermore, the models also predicted that the choking required greater pressure drops when throttle contraction was increased, and that the vapor distribution at choked flow remained almost the same for all the considered throttle configurations (Figure 17). In agreement with the experimental results, the numerical results suggest that contraction does not influence the onset of cavitation or vapor distribution at choked flow, but does influence the development of cavitation, thereby delaying choking.

Table 3 summarizes the pressure drops at which choking occurred for experimental and numerical models. For all three geometries, HRMFoam more accurately predicted the critical onset of choking.

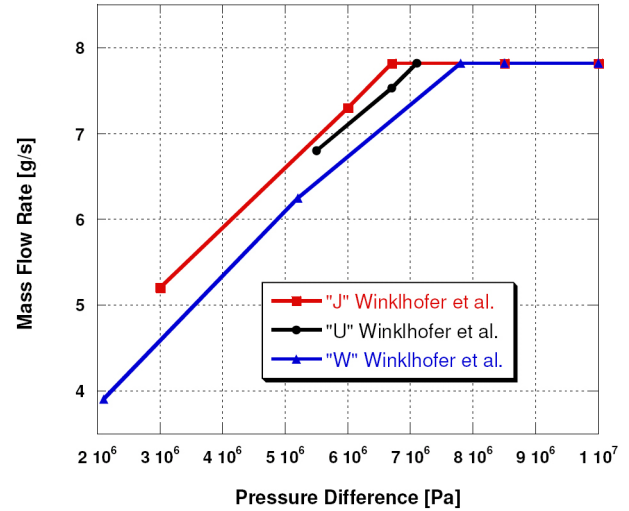


Figure 12. “J”, “U”, and “W” throttle geometries. Experimental mass flow rate evolutions versus pressure drops.

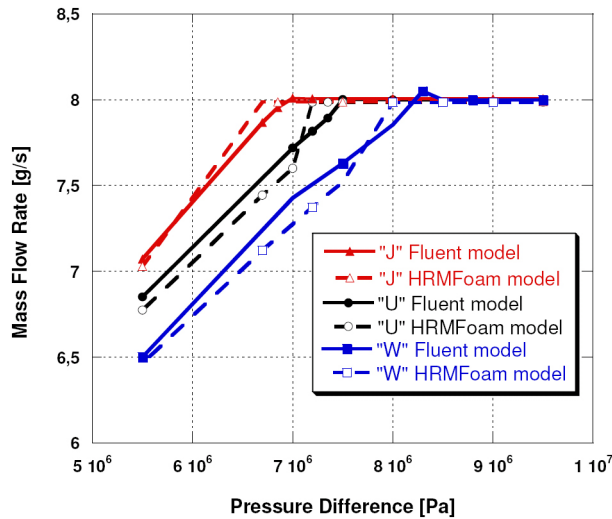


Figure 13. “J”, “U”, and “W” throttle geometries. Numerical mass flow rate evolutions versus pressure drops.

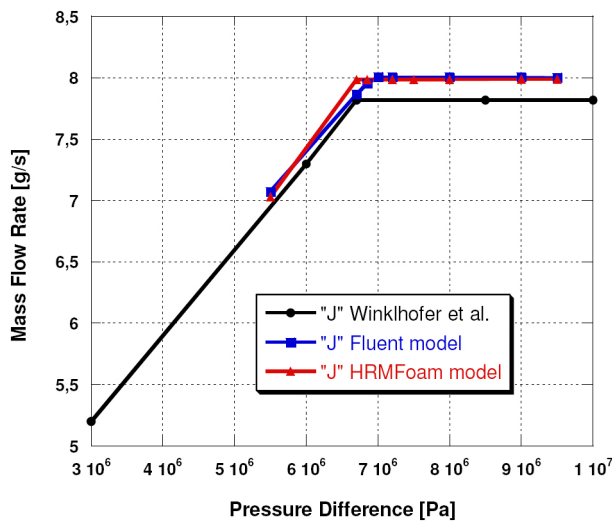


Figure 14. “J” throttle geometry. Comparison between numerical and experimental mass flow rate evolutions versus pressure drops.

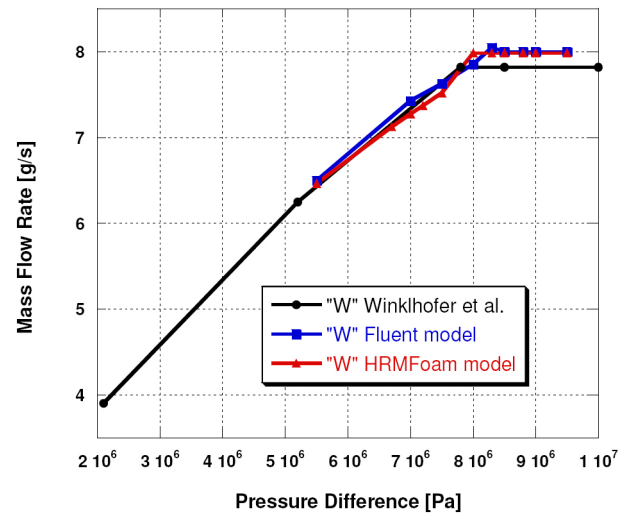


Figure 15. “W” throttle geometry. Comparison between numerical and experimental mass flow rate evolutions versus pressure drops.

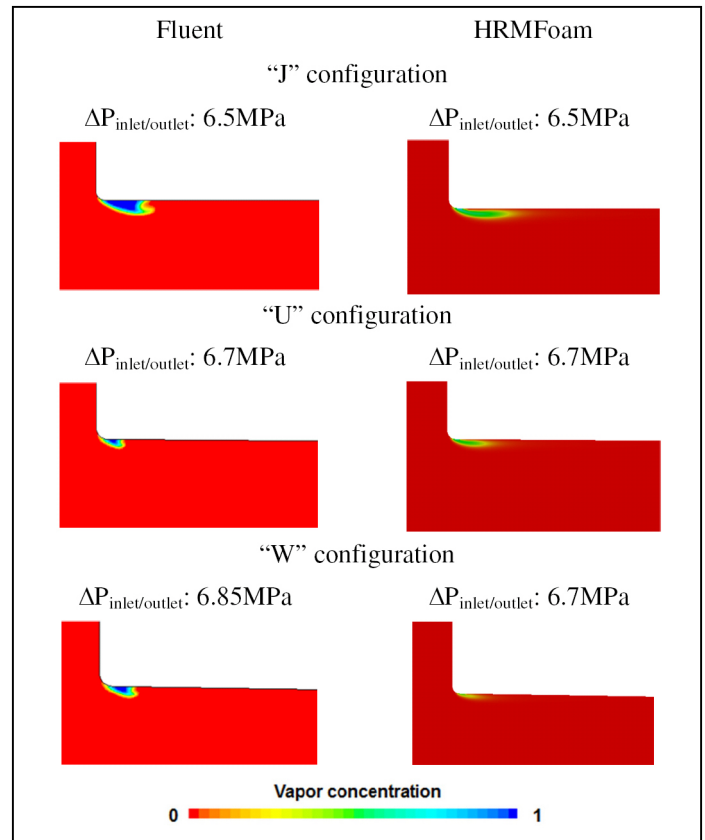


Figure 16. “J”, “U”, and “W” throttle geometries. Vapor distribution at CS condition.

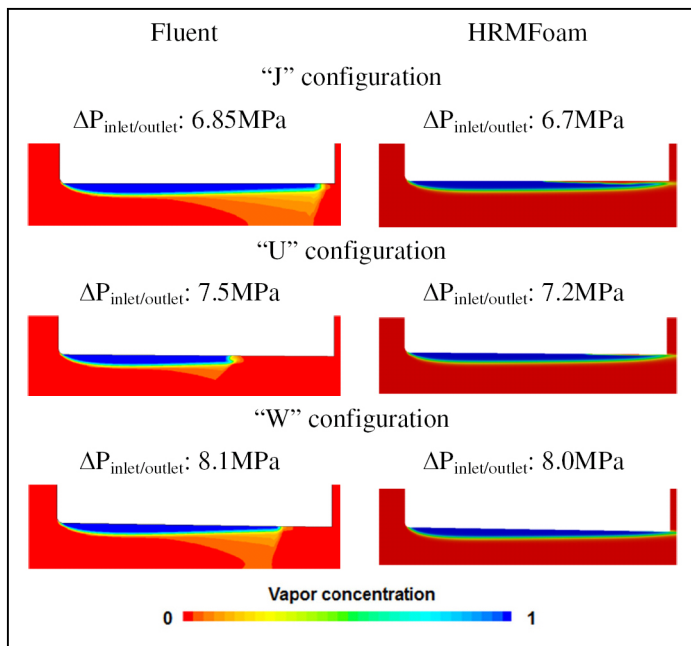


Figure 17. “J”, “U”, and “W” throttle geometries. Vapor distribution at CC condition.

Table 3. Pressure drop corresponding to the CC condition for the “J”, “U”, and “W” throttle geometries.

	ΔP @CC [MPa]		
	Experimental	Fluent model	HRMFoam
“J”	6.5	6.85	6.7
“U”	7.0	7.5	7.2
“W”	7.7	8.1	8.0

CONCLUSIONS

The main goal of the present work was to evaluate and compare the homogeneous relaxation model, originally developed for flash boiling flows, and the Singhal et al. model. The homogeneous relaxation model was implemented in the OpenFOAM framework as HRMFoam, and the Singhal et al. model in Fluent. For comparison, the Winklhofer et al. throttle flow experiments were considered.

The HRMFoam solver was able to correctly predict the initial vapor distribution positioned just downstream the throttle entrance (separation zone) as a function of both the throttle pressure drop and the throttle geometry (“J”, “U”, and “W” throttle configuration). Increasing the throttle pressure drop from the onset of cavitation to fully choked flow, the HRMFoam model predicted a more evident axial propagation and a reduced radial distribution of the void fraction compared to the experimental results. In particular, at choked flow HRMFoam showed the vapor close to the wall while experimental results showed that after choking the liquid stream did not reach the throttle outlet section. It is noteworthy that the two-phase flow is likely to be condensing near the throttle exit, due to the adverse pressure gradient,

and that the HRMFoam solver was conceived for superheated conditions, where vaporization is dominant and condensation is negligible.

With the Fluent cavitation model, the axial extension of the vapor fraction over the pressure drop was closer to the experimental distribution. The radial expansion of cavitation was better predicted by Fluent, although there was still an underestimation compared to the experimental results.

For both models, the predicted evolution of the mass flow rate versus the throttle pressure drop was satisfactorily predicted for all the three throttle configurations. However, the choked mass flow value numerically predicted was slightly higher than the experimental results. This was attributed to the difference in the vaporization pressure value characterizing the experimental Diesel fuel and the Diesel surrogate adopted for the simulation. In all three throttles, the HRMFoam code more accurately predicted the onset of choking than the Singhal et al. model.

The HRMFoam model was able to correctly predict the overall experimental velocities but differences between experimental and numerical data were noticed. At the V_1 location, the velocity gradients recorded by HRMFoam from the throttle wall to the throttle axis were more smoothed than experimental results. This produced a shift in position of the velocity peaks in the shear layer. Despite this, HRMFoam more closely matched the magnitude of the velocity peaks than the Fluent model. In comparison, Fluent was able to better represent the experimental velocity gradient evolution over the radial position but overestimated the peak velocity value. At V_2 , both Fluent and HRMFoam were able to reproduce the experimental velocity distribution in the shear layer and in the center of the throttle, but not the velocity distribution in the transition zone between the liquid phase and the vapor phase (intermediate location between throttle wall and throttle axis). The shortcomings of both numerical models in reproducing the experimental velocity profiles over the liquid/vapor transition zone may be a result of the homogeneous flow approach that assumes an infinitely fast momentum transfer between the liquid and vapor phases.

The simulation results prove the validity of the HRMFoam model to correctly reproduce the main characteristics of cavitating flow through the injector hole as a function of both pressure drop and hole geometry. The Fluent model did not show significant differences with respect to the HRMFoam model. The main differences between the two simulation approaches were the axial vapor distribution close to fully choked flow and the velocity gradient evolution at V_1 .

REFERENCES

1. Mahr, B., "Future and Potential of Diesel Injection Systems", THIESEL 2002 Conference on Thermo- and Fluid-Dynamic Processes in Diesel Engines.
2. Roth, H., Gavaises, M., and Arcoumanis, C., "Cavitation Initiation, Its Development and Link with Flow Turbulence in Diesel Injector Nozzles," SAE Technical Paper [2002-01-0214](#), 2002, doi: [10.4271/2002-01-0214](#).
3. Gavaises, M. and Andriotis, A., "Cavitation Inside Multi-hole Injectors for Large Diesel Engines and Its Effect on the Near-nozzle Spray Structure," SAE Technical Paper [2006-01-1114](#), 2006, doi: [10.4271/2006-01-1114](#).
4. He, L. and Ruiz, F., "Effect of Cavitation on Flow and Turbulence in Plain Orifice for High-Speed Atomization", *Atomization and Sprays*, 1995. 5(6):pp. 569-584.
5. Soteriou, C., Andrews, R.J., Torres, N., Smith, M., and Kunkulagunta, R., "Through the Diesel Nozzle Hole - A Journey of Discovery II". in Proc. ILASSEurope, Zurich, Switzerland, September 2001.
6. Som, S., Aggarwal, S., El-Hannouny, E., and Longman, D., "Investigation of nozzle flow and cavitation characteristics in a diesel injector", *Journal of Engineering for Gas Turbines and Power*, vol. 132, no. 4, 2010.
7. Senda, J., Hojyo, Y., and Fujimoto, H., "Modelling of Atomization Process in Flash Boiling Spray," SAE Technical Paper [941925](#), 1994, doi: [10.4271/941925](#).
8. Schmidt, D. P., Rakshit S., and Neroorkar, K., "Thermal and Inertial Equilibrium in Small, High-Speed, Cavitating Nozzle Simulations," 11th Triennial International Conference on Liquid Atomization and Spray Systems, Vail, Colorado USA, July 2009.
9. Brennen, C. E., "Cavitation and Bubble Dynamics", Oxford University Press, Oxford, 1995.
10. Singhal, A. K., Li, H. Y., Athavale, M. M., and Jiang, Y., "Mathematical Basis and Validation of the Full Cavitation Model", ASME FEDSM'01, New Orleans, Louisiana, 2001.
11. Zwart, P.J., Gerber, A.G., and Belamri, T., "A Two-Phase Flow Model for Predicting Cavitation Dynamics", In Fifth International Conference on Multiphase Flow, Yokohama, Japan, 2004.
12. Neroorkar, K., Shields, B., Grover, R. Jr., Plazas Torres, A. et al., "Application of the Homogeneous Relaxation Model to Simulating Cavitating Flow of a Diesel Fuel," SAE Technical Paper [2012-01-1269](#), 2012, doi: [10.4271/2012-01-1269](#).
13. Gopalakrishnan, S. and Schmidt, D., "A Computational Study of Flashing Flow in Fuel Injector Nozzles," *SAE Int. J. Engines* 1(1):160-170, 2009, doi: [10.4271/2008-01-0141](#).
14. Neroorkar, K., "Modeling of Flash Boiling Flows in Injectors with Gasoline-Ethanol Fuel Blends". PhD thesis, The University of Massachusetts-Amherst, 2011.
15. Neroorkar, K. and Schmidt, D., "A Computational Investigation of Flash-Boiling Multi-hole Injectors with Gasoline-Ethanol Blends," SAE Technical Paper [2011-01-0384](#), 2011, doi: [10.4271/2011-01-0384](#).
16. Winklhofer, E., Kull, E., Kelz, E., and Morozov, A., "Comprehensive hydraulic and flow field documentation in model throttle experiments under cavitation conditions," 17th Annual Conference on Liquid Atomization and Spray Systems, Zurich, Switzerland, September 2001.
17. Weller, H., Tabor, G., Jasak, H., and Fureby, C., "A tensorial approach to computational continuum mechanics using object-oriented techniques", *Computers in Physics*, vol. 12, no. 6, pp. 620-631, 1998.
18. Schmidt, D. P., "Cavitation in Diesel Fuel Injector Nozzles". PhD thesis, The University of Wisconsin-Madison, 1997.
19. Negro, S., Brusiani, F., and Bianchi, G., "Superheated Sprays of Alternative Fuels for Direct Injection Engines," SAE Technical Paper [2012-01-1261](#), 2012, doi: [10.4271/2012-01-1261](#).
20. Negro, S., Brusiani, F., and Bianchi, G., "A Numerical Model for Flash Boiling of Gasoline-Ethanol Blends in Fuel Injector Nozzles," *SAE Int. J. Fuels Lubr.* 4(2):237-256, 2011, doi: [10.4271/2011-24-0003](#).
21. Downar-Zapolski, P., Bilicki, Z., Bolle, L., and Franco, F., "The Non-Equilibrium Relaxation Model for One-Dimensional Flashing Liquid Flow," 3rd ASME/JSME Joint Fluids Engineering Conference, vol. 208, no. 616, 1999.
22. Schmidt, D., Gopalakrishnan, S., and Jasak, H., "Multidimensional Simulation of Thermal Non-Equilibrium Channel Flow," *Intl. J. of Multiphase Flow*, vol. 36, pp. 284-292, 2010.
23. Reocreux, M., "Contribution a letude des debits critiques en ecolement diphasique eau-vapeur", PhD thesis, Universite Scientifique et Medicale de Grenoble, France 1974.
24. Versteeg, H.K., Malalasekera, W., "An Introduction to Computational Fluid Dynamics: The Finite Volume Method" (2nd edition), Longman, 2006.
25. Launder, B. E. and Spalding, D. B., "The Numerical Computation of Turbulent Flows", *Computer Methods in Applied Mechanics and Engineering*, 3:269-289, 1974.
26. Weber, J., Peters, N., Diwakar, R., Siewert, R. et al., "Simulation of the Low-Temperature Combustion in a Heavy Duty Diesel Engine," SAE Technical Paper [2007-01-0904](#), 2007, doi: [10.4271/2007-01-0904](#).

ACKNOWLEDGMENTS

Authors would like to thank Dr. Ernst Winklhofer for providing the experimental pictures and the velocity profiles

used in the present work to test the cavitation models. The financial support of General Motors Research Center is acknowledged.

$\bar{\tau}$ - Shear stress.
 t - Time.

DEFINITIONS/ABBREVIATIONS

GDI - Gasoline Direct Injection.

CR - Common-Rail.

RANS - Reynolds-averaged Navier-Stokes.

CS - Cavitation starting point.

CC - Cavitation chocking condition.

NOMENCLATURE

ρ - Mixture density.

ρ_l - Liquid density.

ρ_v - Vapor density.

f - Vapor mass fraction.

α - Void fraction.

n - Bubble number density.

R_B - Bubble radius.

P - Pressure.

P_B - Bubble pressure.

P_v - Vapor pressure.

P'_{turb} - Turbulent pressure fluctuation

Rc - Condensation source term.

Re - Evaporation source term.

k - Turbulent kinetic energy.

ε - Turbulent dissipation rate.

I - Turbulence intensity.

l - Turbulence length scale.

\vec{U} - Velocity vector.

h - Enthalpy.

x, \bar{x} - Instantaneous and equilibrium mass fractions respectively.

ϕ, ϕ_v - Mass flux and volumetric flux respectively.

θ - Vaporization time scale.

The Engineering Meetings Board has approved this paper for publication. It has successfully completed SAE's peer review process under the supervision of the session organizer. This process requires a minimum of three (3) reviews by industry experts.

All rights reserved. No part of this publication may be reproduced, stored in a retrieval system, or transmitted, in any form or by any means, electronic, mechanical, photocopying, recording, or otherwise, without the prior written permission of SAE.

ISSN 0148-7191

Positions and opinions advanced in this paper are those of the author(s) and not necessarily those of SAE. The author is solely responsible for the content of the paper.

SAE Customer Service:

Tel: 877-606-7323 (inside USA and Canada)

Tel: 724-776-4970 (outside USA)

Fax: 724-776-0790

Email: CustomerService@sae.org

SAE Web Address: <http://www.sae.org>

Printed in USA